# Pore Size Distributions in Low-*k* Dielectric Thin Films from X-ray Porosimetry*

**HAE-JEONG LEE, CHRISTOPHER L. SOLES, DA-WEI LIU, BARRY J. BAUER, WEN-LI WU**

Polymers Division, MSEL, National Institute of Standards and Technology (NIST), 100 Bureau Drive, Mail Stop 8541, Gaithersburg, Maryland 20899

*Received 28 May 2002; revised 28 June 2002; accepted 28 June 2002*

**ABSTRACT:** X-ray reflectivity has been used to determine the mass uptake of probe molecules in porous thin films supported on thick silicon wafers. The adsorption occurs by capillary condensation when the films are exposed to probe vapor at controlled partial vapor pressures. The probe solvent partial pressure was varied by mixing saturated air and dry air at constant temperature or by changing sample temperature at a constant vapor concentration. Pore size distribution in the films can be calculated from the probe uptake with typical porosimetric approaches such as the application of the Kelvin equation to convert partial pressure into pore size. For illustration, the pore size distribution of three different nanoporous thin films, the primary candidate of ultra-low-*k* interlevel dielectrics in the next generation of integrated circuit chips, was determined with this technique. These samples represent different generations of low-*k* dielectrics developed by industry. © 2002 Wiley Periodicals, Inc. J Polym Sci Part B: Polym Phys 40: 2170–2177, 2002

**Keywords:** X-ray; thin films; particle size distribution; adsorption

## INTRODUCTION

The rapid and sustained advances in ultra-large-scale integrated circuit performance have been driven, to a large extent, by miniaturization of the circuitry. Predictions from the semiconductor industry indicate that by 2003, 100-nm nodes will be realized.[1] At these dimensions, interlayers with extremely low dielectric constants (low-*k*) are imperative to reduce cross-talk and to increase processor speed. It is estimated that 100-nm technology nodes will require interlevel metal insulators with a bulk dielectric constant $k = 2.2$ or below,[1] which is significantly less than the silica-based insulators ($k = 4.3$) that were the industrial standard four years ago. However, the past four years have also witnessed significant materials advances, and there are now alternate systems capable of meeting the desired level of $k = 2.2$. Although the candidate materials differ in their base chemistries (i.e., $SiO_2$, $RSiO_{1.5}$, SiCOH, hydrocarbons, etc.), a common theme emerges in the push to develop low-*k* dielectric materials—nanoscale porosity must be introduced in a controlled manner to further reduce *k*. The emphasis on controlled porosity is critical given that the lateral dimensions or the feature size of the interlayer dielectric films are less than 100 nm. It is desirable to keep the pore dimensions at least one order of magnitude smaller than the feature size to minimize catastrophic film defects and/or pore architectures that could lead to shorting via Cu ion migration or dielectric breakdown.

*Contribution from the March 2002 Meeting of the American Physical Society—Division of Polymer Physics, Indianapolis, Indiana

*Correspondence to:* B. J. Bauer (E-mail: barry.bauer@nist.gov)

Journal of Polymer Science: Part B: Polymer Physics, Vol. 40, 2170–2177 (2002)

One attractive approach to creating controlled pore architectures is to formulate the spin-on low-*k* dielectric precursor solution with porogens that can be polymers or other organic materials. After high-temperature processing, the polymer or organic porogens volatilize leaving a porous structure. Techniques are needed to accurately and noninvasively characterize the porosity (pore size, distribution, volume, etc.) in these films attached on a silicon substrate. In this article we demonstrate how specular X-ray reflectivity (SXR) can be used to obtain detailed porosity information in nanoporous low-*k* dielectric films attached to silicon substrate.

Traditional porosimetric techniques, such as $N_2$ adsorption, mercury intrusion, or quartz crystal microbalances, lack the sensitivity to characterize the porosity in films that are less than 1 $\mu$m thick and still attached to a 1-mm-thick silicon single-crystal wafer. There are, however, a few relatively new techniques capable of quantifying aspects of the pore structure in low-*k* dielectric films *in situ*, or directly on the wafer. For example, we have shown that a combination of neutron scattering, ion-beam scattering, and X-ray reflectivity experiments can elucidate detailed pore information, such as porosity and the average pore size.[2,3] The applicability of this methodology is, however, limited because neutron scattering is not a laboratory-scale facility. Attractive alternatives for measuring pore sizes in thin films include the positron beam techniques (lifetime spectroscopy and Doppler broadening measurements) that are especially useful for characterizing the very smallest pores (i.e., 2–20 Å in diameter).[4–7] However, commercial positron beams are not readily available.

Recently, ellipsometric porosimetry (EP) has emerged as a powerful technique for mapping out pore size distributions in porous thin films.[8] EP is similar to $N_2$ adsorption in that the sample is exposed to a gaseous adsorbate or probe molecule. As the partial pressure increases, the gas condenses into increasingly larger pores via capillary condensation. Although the $N_2$ adsorption isotherms infer the amount of adsorbed gas from changes in the partial pressure, EP monitors adsorption (usually of an organic solvent vapor) through changes in the film's index of refraction. The EP methodology provides an attractive alternative for the semiconductor industry as the instrumentation can be readily implemented. There are, however, concerns regarding the EP technique. Now the working assumption for EP is the additivity of the polarizability of the constituents. Furthermore, it also assumes that the index of refraction of a condensed liquid (e.g., toluene) in a nanoscale pore is identical to that of the bulk liquid. It is not immediately obvious if these assumptions are reasonable when the pore size approaches that of a few adsorbate molecules.

In the following, we introduce a X-ray reflectivity version of EP that we refer to as X-ray porosimetry (XRP). As with EP, the chemical potential of an organic solvent vapor is slowly increased to induce condensation of vapor into increasingly larger pores. In XRP this uptake is directly quantified in terms of the mass uptake from the reflection critical angle without invoking any assumption. The critical angle is defined as the grazing angles below which total reflectance of an X-ray beam occurs. This critical angle $\theta_c$ depends on the electron density $\rho_e$ (and thus mass density) of the film through

$$\theta_c = \lambda(\rho_e r_e/\pi)^{0.5} \tag{1}$$

where $\lambda$ is the X-ray wavelength, and $r_e$ is the classical electron radius. As condensation into a pore results in a significant change of the overall film density, changes in $\theta_c$ are an accurate measure of the adsorbate uptake. We emphasize that this technique does not require assumptions regarding neither the additivity of polarizability nor the optical properties or other material parameters that might be susceptible to confinement-induced changes. If the chemical compositions of the adsorbate or the probe molecule are known, the changes in $\theta_c$ are directly related to the mass uptake per unit volume.

It is common to analyze condensation data in porous media in terms of the Kelvin equation. At pressures below saturation, it is possible to condense liquid in small pores via the mechanism of capillary condensation. The Laplace pressure from the curvature of the meniscus inside the condensed pore shifts the liquid-vapor equilibrium, making condensation feasible at partial pressures much lower than equilibrium vapor pressure. The pore size $r_k$ for capillary condensation is typically described by the Kelvin equation

$$r_k = \frac{2V_m\gamma}{-RT}\frac{1}{\ln(P/P_0)} \tag{2}$$

where $\gamma$ is the liquid surface tension, $V_m$ is the molar volume of the liquid, $P$ is the partial pres-

sure, and $P_0$ is the equilibrium pressure over a flat liquid surface at a temperature $T$. The Kelvin equation provides a simple relationship between the pore size and partial pressure; when combined with the mass-uptake data, it provides a powerful tool to determine the pore size distribution within a porous medium. The use of the Kelvin equation to calculate pore size invokes many approximations, and clearly, as the pore size approaches that of the adsorbate or probe molecules, the Kelvin relationship will fail. It is beyond the scope of this work to discuss various modifications and improvements made by many investigators in porosimetry. The objective of this work is to demonstrate the applicability of X-ray reflectivity as a powerful tool to determine mass uptake of an adsorbate into thin films while attached to a thick substrate.

In this article we demonstrate how SXR can be used to generate a capillary condensation isotherm for several industrially relevant low-$k$ dielectric films. In lieu of a better alternative, we naively apply the Kelvin equation to approximate the pore size distributions. Although this pushes the analysis into a regime where the assumptions behind the Kelvin equation are clearly not valid, the qualitative differences between the different types of low-$k$ dielectric films are robust. Furthermore, the Kelvin equation is routinely used with the EP technique (despite the limitations), and presenting our data in the same format will facilitate a comparison between the two techniques.

## EXPERIMENTAL

Two techniques were used to vary the chemical potential, that is, $P/P_0$ of the toluene vapor that the low-$k$ dielectric films were exposed to. In the first method, $P/P_0$ is varied isothermally by changing the partial pressure, $P$, of the toluene. First, the sample was evacuated in the reflectometer at 175 °C for 2 h. Then the chamber was backfilled and purged with dry air to establish a toluene partial pressure of zero. After collecting the reflectivity at $P/P_0 = 0$, small aliquots of toluene-saturated air were injected into the chamber with a glass syringe. The air with toluene saturation was produced by slowly bubbling dry air through toluene liquid at room temperature. Approximately 30 min after each injection, the reflectivity data were collected, and the partial pressure of the toluene was measured via UV absorption. This procedure was repeated until the vapor pressure of the sample chamber reached saturation, creating an adsorption isotherm. The desorption branch of the isotherm was then generated by diluting the toluene content of the sample chamber through dry-air injections. These dry-air injections were repeated, collecting both the reflectivity and UV adsorption in an analogous manner, until the partial pressure of toluene was nearly zero. To measure the partial pressure, a UV–visible quartz absorption cell with a 10-mm path length was connected to the sample chamber. Immediately following each reflectivity measurement, the valves to the quartz cell and the sample chamber were closed off to prevent exchange between the sample environment and the external atmosphere. The quartz cell was then removed, and the UV absorption was measured between 200 and 280 nm on a PerkinElmer UV-VIS spectrometer.[9] The partial pressure was easily determined by integrating the peak heights for the strong toluene band at 258 nm. After collecting the absorption data, the quartz cell was reconnected and allowed to equilibrate with the sample environment. The relative uncertainty of the UV adsorption and the vapor concentrations calculated from them are in the range of ±10% on the basis of repeated measurements of typical samples. The uncertainties are not shown in the figures for clarity.

In the second method, a constant stream of air with toluene saturation was passed over the sample. The dry air was saturated by bubbling through liquid toluene at (20 ± 0.1) °C at a rate of approximately 2 mL/min. The $P/P_0$ ratio was then varied by changing the sample temperature from 20 to 125 °C, with a stability of ±0.1 °C. After each temperature change (variable increments), the reflectivity was obtained after 30 min of thermal equilibration. In this mode of operation, the equilibrium saturation pressure $P_0$ changes with temperature, whereas $P$ remains constant (heating corresponds to the desorption, and cooling corresponds to the adsorption).

X-ray reflectivity measurements were performed on a diffractometer with a $\theta$-$2\theta$ configuration. The incident beam of Cu K$\alpha$ radiation, $\lambda = 1.54$ Å, was directed with a focusing mirror into a four-bounce Ge (220) crystal monochromator. After reflecting from the film, the beam was collected with a three-bounce channel-cut Ge (220) crystal and directed into a solid-state detector. The angular reproducibility of this goniometer was ±0.0001° and is taken as the standard uncertainty in this measurement. After each $P/P_0$

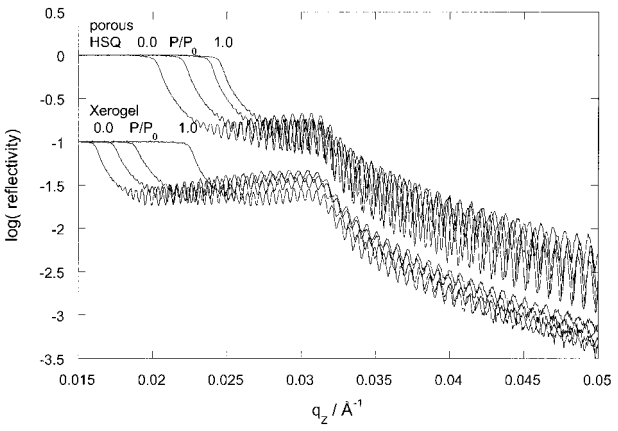


**Figure 1.** X-ray reflectivity curves for the Xerogel and porous HSQ samples at various $P/P_0$ values of toluene at 20 °C (top curve, porous HSQ; bottom curve, Xerogel; left-most curve, $P/P_0 = 0$; and right-most curve, $P/P_0 = 1$).

increment, 30 min were allowed for equilibration, and the reflectometer was always realigned before collecting data.

To demonstrate the utility of XRP, we chose to examine three typical low-$k$ dielectric films. The first was a sol–gel silica material produced from TEOS precursors, identified as "Xerogel"-type material. The second film was a spin-on hydrogen silsesquioxane based on porous film, and the third film was an organsilsesquioxane resin formulated with a polymeric porogen. These are identified as "porous HSQ"-type material and "porous MSQ"-type material, respectively.

## RESULTS

The reflectivity $R$ ($R = I_{\text{reflected}}/I_{\text{incident}}$), where $I$ is beam intensity, from the porous HSQ and the Xerogel films is shown in Figure 1. Each of the two samples has several data sets plotted together to show the effect of solvent adsorption. The critical edge is clearly visible as the sharp drop in log($R$) from the initially flat reflectivity curve. In Figure 1 four curves are displayed for each sample, varying from the sample exposed to dry air (left-most curve) to sample in saturated toluene vapor (right-most curve). There is a progression of the critical edge to higher $q$ as the vapor pressure increases because of the increased electron density of the film as the smaller pores become saturated with liquid toluene. The curve is fit[10] to produce a value of the critical edge that is then converted to electron density by eq 1.

The atomic composition is necessary to convert the electron density to mass density. If this is not known *a priori* (as is the case here), a combination of forward recoil elastic scattering and Rutherford backscattering can be used to measure the film atomic composition, as described previously.[2,3] Table 1 summarizes the atomic composition for the three films reported in this work.[11] If the film is not swollen by toluene, then the electron density determined from the critical edges of the dry and the toluene-infiltrated films can be used to calculate the mass uptake of toluene. By further assuming the density of the toluene is the same as the bulk, as is the practice of other thin-film measurements,[8] the total open pore-volume fraction and the average mass density of the wall and closed pores can be calculated. If the density of toluene in confined, small pores is higher than bulk toluene, this will slightly underestimate the pore volume. Table 2 gives the densities and porosities of the three samples. In these calculations, the mass density of toluene at 20 °C that was used was 0.865 g/cc, giving an electron density of 0.283 electrons/Å$^3$.

At $P/P_0 = 1$, toluene will condense in all of the accessible pores or open pores by definition so the uptake at saturation, $W_0$, is a measure of the porosity. The porosities based on these maximum uptake values are reported in Table 2. This porosity only reflects those pores that the toluene can infiltrate. There may also be closed pores not accessible to toluene vapor and therefore not reflected in the XRP porosity. Therefore, a matrix density that is a combination of dense-wall mate-

**Table 1.** Atomic Compositions of the Xerogel, Porous HSQ, and Porous MSQ Films Described in This Article

| Sample | H (atomic %) | C (atomic %) | O (atomic %) | Si (atomic %) |
|---|---|---|---|---|
| Xerogel | 33 ± 5 | 14 ± 5 | 34 ± 5 | 19 ± 5 |
| Porous HSQ | 20 ± 5 | 7 ± 5 | 48 ± 5 | 25 ± 5 |
| Porous MSQ | 47 ± 5 | 15 ± 5 | 23 ± 5 | 15 ± 5 |

**Table 2.** SXR Results of Samples in Table 1 with Calculated Density and Porosity Values

| Sample | $q_c$ ($10^{-4}$ Å$^{-2}$) | $\rho_{electron}$(e$^-$/Å$^3$) | $\rho_{mass}$ (g/cm$^3$), Film Density | $\rho_{mass}$ (g/cm$^3$), Matrix + Closed Pores | Open Pore Porosity |
|---|---|---|---|---|---|
| Xerogel | 2.65 ± 0.10 | 0.187 ± 0.007 | 0.605 ± 0.023 | — | — |
| + Toluene | 5.11 ± 0.10 | 0.361 ± 0.007 | — | 1.136 ± 0.023 | 0.614 ± 0.05 |
| Porous HSQ | 4.30 ± 0.10 | 0.303 ± 0.007 | 0.995 ± 0.023 | — | — |
| + Toluene | 6.08 ± 0.10 | 0.429 ± 0.007 | — | 1.379 ± 0.023 | 0.444 ± 0.015 |
| Porous MSQ | 3.95 ± 0.10 | 0.279 ± 0.007 | 0.886 ± 0.024 | — | — |
| + Toluene | 5.30 ± 0.10 | 0.374 ± 0.007 | — | 1.177 ± 0.024 | 0.337 ± 0.05 |

rial and inaccessible closed pores can be calculated. In principle, if the wall density is precisely known by some other means, the closed-pore content can be determined from the difference between the actual and calculated matrix densities.

Figure 2 demonstrates how the partial pressure $P/P_0$ can be measured from the UV absorption of the vapor in the sample chamber of the reflectometer. A series of curves are shown where $P/P_0$ is varied from 0 to 1, clearly demonstrating that the 10-mm path length of the quartz cell is sufficient to register changes in the vapor composition. The partial pressure can be calculated from absorption at 258 nm, using the conditions of the dry air and completely saturated toluene as the normalizing end points.

Figure 3 depicts the $P/P_0$ versus $W/W_0$ variations for the porous HSQ and the Xerogel films. Both curves exhibit a hysteresis between the adsorption and desorption branches of the isotherms; this is a hallmark of the capillary condensation mechanism. The strong increase (or decrease) in uptake at moderate partial pressures occurs when the toluene molecules condense (or evaporate) in the pores of the low-$k$ films. That the adsorption/desorption occurs at higher partial pressures in the Xerogel film than as compared with the porous HSQ film indicates larger pores in the Xerogel film. A pore size distribution can be determined from the derivative of the adsorption/desorption isotherms, with the $P/P_0$ axis recast in terms of the critical pores size for capillary condensation (Kelvin equation).

To facilitate the pore size distribution calculations, it is helpful to fit a smooth function to the isotherms in Figure 3, as a point-by-point differentiation leads to considerable scatter. In Figure 4 the desorption isotherms are arbitrarily fit with a Gaussian of variable width and height (for clarity the adsorption isotherms are omitted). The Gaussian function does a reasonable job at parameterizing the data, falling well within the uncertainty limits. Then the corresponding pore size distributions given in Figure 5 determine both the Gaussian fits as well as the point-by-point

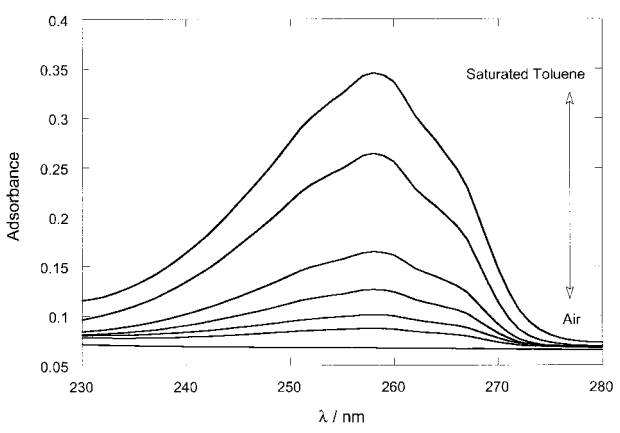


**Figure 2.** UV adsorption of captured toluene vapor in a 10-mm quartz cell (top curve, $P/P_0$ = 1 and bottom curve, $P/P_0$ = 1).

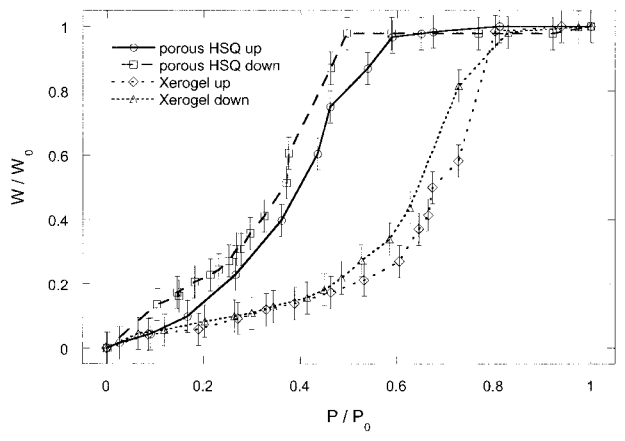


**Figure 3.** $P/P_0$ versus $W/W_0$ data for porous HSQ and Xerogel films during $P/P_0$ increase (filling) and $P/P_0$ decrease (emptying).

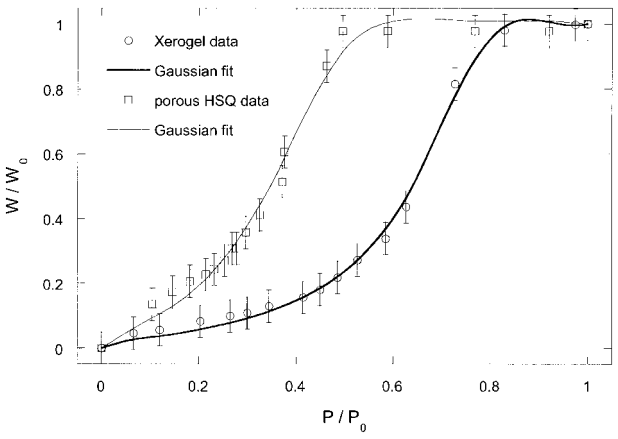


**Figure 4.** $P/P_0$ versus $W/W_0$ data for porous HSQ and Xerogel films during $P/P_0$ decrease (emptying) and fits to Gaussian pore size distribution.

differentiation. The means and widths of the distributions reported in Table 3 according to the equation

$$P(R) = \exp\left[-\left(\frac{R - \langle R \rangle}{\sigma}\right)^2\right] \tag{3}$$

where $\langle R \rangle$ is the average pore size, and $\sigma$ is the width of the distribution.

The pore sizes in Figure 5 and Table 3 are in the range where interactions between the toluene and the pore surface may be significant. The diameter of a toluene molecule is approximately 6 Å, and it has been shown that near a surface there is a pronounced structural layering of toluene that extends for 4–5 molecular diameters, or tens of Å.[12] The length scale of this layering is comparable to the pore dimensions reported in Figure 5 and Table 3. As surface-induced liquid layering dramatically increases the viscosity of a liquid,[13] one must also consider the possibility that the equilibrium between the liquid and the vapor is also affected. In this respect, the meniscus curvature may not be the factor affecting the capillary condensation mechanism, and absolute values of the pore sizes may therefore not be precise. However, the differences between the adsorption/desorption isotherms and the various films still reflect important characteristics of the pores.

The first feature worth noting in Figure 5 and Table 3 is that the average pore sizes are larger when calculated from the filling (increasing pressure) rather than the emptying (decreasing pressure) portions of the hysteresis loop. This is normal for the capillary condensation mechanism, as discussed in detail elsewhere.[14] In the ideal situation of cylindrical pores of a single diameter, the width of the pore size distribution from the adsorption and desorption isotherms should be similar. The fact that the width of the distribution is broader when calculated from the filling (increasing pressure) branch of the hysteresis loop as opposed to the emptying (decreasing pressure) branch suggests that there is a distribution of pore sizes. Pore-blocking effects can prevent the larger pores from draining, in which case the average pore size on desorption is weighted toward the minimum or restricting pore diameter. However, as will be demonstrated shortly, the differences between the adsorption and desorption isotherms are relatively small in Figure 5, and the pore-blocking effects are probably minimal. In comparing the different films in Figure 5, we see that Xerogel has larger pores, a broader distribution of pore sizes, and a greater overall porosity than the porous HSQ film. The larger porosity is consistent with the lower dielectric constant observed in the Xerogel film.

The examples of the Xerogel and porous HSQ were true isotherms in that the partial pressure was varied while maintaining a constant temperature. This mode of data collection is somewhat tedious with our apparatus; the vapor pressure is manually changed by injecting aliquots of either toluene saturated or dry air into the sample chamber, and then capturing a small volume of the atmosphere to measure the UV absorption on an external spectrometer. This method is prone errors because of the necessity of physically moving a captured volume of the atmosphere to a UV

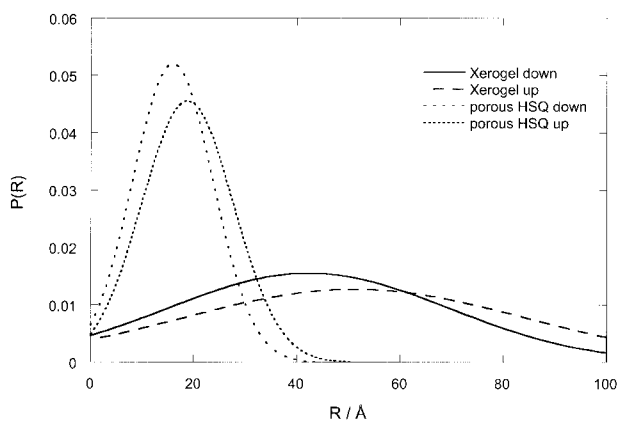


**Figure 5.** Fits of Gaussian pore size distribution of samples shown in Figure 3.

**Table 3.** Fits of $P/P_0$ versus $W/W_0$ Data to Gaussian Pore Size Distribution as Determined by Eq 3

| Sample | Loop | ⟨R⟩/Å | σ/Å |
|---|---|---|---|
| Xerogel | Up (filling) | 51.2 ± 1.6 | 33.3 ± 3.3 |
| Xerogel | Down (emptying) | 42.3 ± 0.7 | 27.2 ± 1.5 |
| Porous HSQ | Up (filling) | 18.8 ± 0.3 | 8.9 ± 0.5 |
| Porous HSQ | Down (emptying) | 15.9 ± 0.2 | 7.8 ± 0.5 |
| Porous MSQ | Up (filling) | 34.0 ± 1.3 | 16.5 ± 1.2 |
| Porous MSQ | Down (emptying) | 21.4 ± 0.2 | 2.0 ± 0.2 |

spectrometer several times to create a single isotherm and is the primary cause of the scatter in the data of Figure 3. We are in the process of building an automated apparatus that incorporates metering pumps to control the toluene content of the sample chamber and then measures of the UV absorption *in situ*.

In lieu of an automated device to carefully control and measure the partial pressure of the toluene, an alternative method was devised to vary to chemical potential of the toluene, or $P/P_0$. By maintaining a fixed concentration of solvent, $P$, in the cell, it is possible to vary the saturation pressure $P_0$ by changing the temperature. From a thermodynamic point of view, there should be no difference whether $P$ or $P_0$ is varied in eq 2 (as long as spinodal condensation and/or evaporation does not occur,[15] in which case the Kelvin equation would also be in serious error). We revisit this temperature-pressure equivalency question once the automated pressure control device is in place. The temperature, or $P_0$, variations provide an attractive alternative because $P/P_0$ can be calculated from the sample temperature, and it is not necessary to measure $P/P_0$, which increases both the speed and accuracy of the measurements.

Figure 6 presents the adsorption/desorption data for the porous MSQ film in which $P/P_0$ is varied through the substrate temperature. The solid lines are cubic splines through the data and accurately mimic the shape of the curves. It is clear that the data points have considerably less scatter than the data in Figure 3 where the isothermal technique was used. The hysteresis loop is very well defined with data outside of the loop coinciding accurately. If the principle of temperature-pressure equivalency is valid, then the temperature-control method clearly increases the accuracy with our existing equipment.

The increased quality of the data in Figure 6 makes it reasonable to calculate the pore size distribution from a point-by-point differentiation, as shown in Figure 7. However, despite the apparently smooth variations in Figure 6, the point-by-point transformation increases the noise and

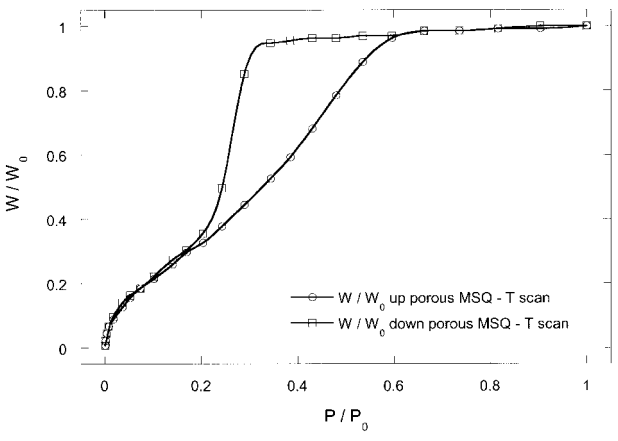


**Figure 6.** $P/P_0$ versus $W/W_0$ data for porous MSQ film during $P/P_0$ increase (filling) and $P/P_0$ decrease (emptying).

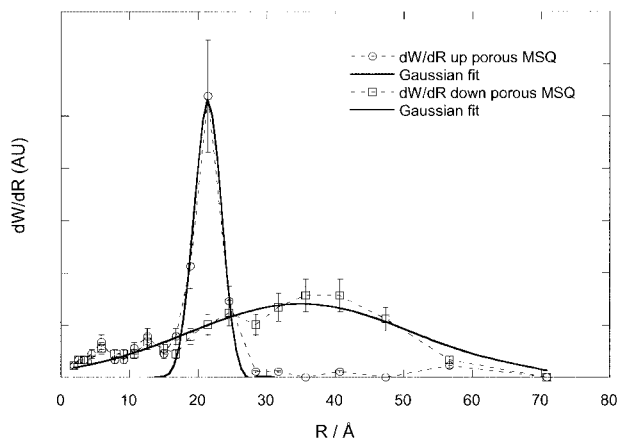


**Figure 7.** Fits of incremental and Gaussian pore size distributions for a porous MSQ sample shown in Figure 3.

still gives the data a somewhat erratic nature. As with the porous HSQ and Xerogel, a single Gaussian reasonably fits the pores size distribution for both the adsorption and desorption pathways, as demonstrated in Figure 7. The corresponding Gaussian amplitude and width are reported in Table 3 in conjunction with the Xerogel and porous HSQ data. Both techniques consistently show a larger pore size and broader pore distributions for the filling branch of the hysteresis loop, as expected for capillary porosimetry.

There are several advantages of XRP over many other techniques to determine pore size in ultrathin films. Some methods require that the film be deposited on a special substrate, such as the piezoelectric surfaces required for both the quartz crystal microbalance and surface acoustic waves techniques. XRP can be done on any smooth substrate, including the Si wafers used in the semiconductor industry. In many ways, XRP is similar and complimentary to EP. However, the EP analysis requires knowledge of the optical constants for both the matrix and the adsorbate. With EP it is also necessary to invoke the additional assumption that the polarizabilities are additive. XRP does not require these additional assumptions. Although the film's atomic content can be accurately transformed into electron density, the refractive index depends on both the atomic content and the nature of the chemical bonds.

Another potential advantage of XRP is the ability to quantify not only the average film density but also the density profile normal to the film surface. Examples of using X-ray reflectivity to extract nonuniform density profiles in a series of low-$k$ film are documented elsewhere.[16] In principle, XRP could be used to extract pore size distributions as a function of both $P/P_0$ and depth into film. To prevent dielectric breakdown it is desirable to have low porosity or very small pores near the surfaces with the majority of the porosity in the localized center of the thin film. XRP could prove to be very useful for characterizing these types of structures.

Finally, the instrumentation required for XRP is readily available and easily implemented in any laboratory of fabrication facility. Most X-ray diffractometers can perform reflectivity measurements with little or no modification. In this respect, XRP provides an accurate and easy methodology for measuring pore size distribution in thin dielectric films to be used either in place of or in conjunction with competing techniques.

This work was supported in part by the Office of Microelectronics Program at NIST. The authors are also indebted to Jeffrey Lee, Jeff Wetzel, and Michael Gallagher for providing the samples. The authors are also grateful to Russ Composto and Doug Yates of the University of Pennsylvania for their assistance in the RBS and FRES measurements.

## REFERENCES AND NOTES

1. International Technology Roadmap for Semiconductors; Semiconductor Industry Association: Gaithersburg, MD, 2001.
2. Bauer, B. J.; Lin, E. K.; Lee, H. J.; Wang, H.; Wu, W. L. J Electron Mater 2001, 30, 304.
3. Wu, W.-L.; Wallace, W. E.; Lin, E. K.; Lynn, G. W.; Glinka, C. J.; Ryan, E. T.; Ho, H. M. J Appl Phys 2000, 87, 1193.
4. Petkov, M. P.; Weber, M. H.; Lynn, K. G.; Rodbell, K. P.; Cohen, S. A. Appl Phys Lett 1999, 74, 2146.
5. Gidley, D. W.; Freize, W. E.; Dull, T. L.; Sun, J.; Yee, A. F.; Nguyen, C. V.; Yoon, D. Y. Appl Phys Lett 2000, 76, 1282.
6. Sun, J.; Gidley, D. W.; Dull, T. L.; Frieze, W. E.; Yee, A. F.; Ryan, E. T.; Lin, S.; Wetzel, J. J Appl Phys 2001, 89, 5138.
7. Dull, T. L.; Frieze, W. E.; Gidley, D. W.; Sun, J. N.; Yee, A. F. J Phys Chem B 2001, 105, 4657.
8. Baklanov, M. R.; Mogilnikov, K. P.; Polovkinkin, V. G.; Dultsev, F. N. J Vac Sci Technol B 2000, 18, 1385.
9. Certain commercial materials and equipment are identified in this article to specify adequately the experimental procedure. In no case does such identification imply recommendation by the National Institute of Standards and Technology (NIST), nor does it imply that the material or equipment identified is necessarily the best available for this purpose.
10. Anker, J. F.; Majkrzak, C. J. In Neutron Optical Devices and Applications; SPIE Proceedings 1738; SPIE: Bellingham, WA, 1992; p 260.
11. All data in the tables and figures are presented with the standard uncertainty (±) associated with the measurement.
12. Klein, J.; Kumacheva, E. J Chem Phys 1998, 108, 6996.
13. Granick, S. Science 1991, 253, 1374.
14. Rouquerol, F.; Rouquerol, J.; Sing, K. Adsorption by Powders and Porous Solids: Principles, Methodology, and Applications; Academic: London, 1999.
15. Neimark, A.; Ravikovitch, P. I.; Vishnyakov, A. Phys Rev E: Stat Phys Plasmas Fluids Relat Interdiscip Top 2000, 62, R1493.
16. Lee, H. J.; Lin, E. K.; Wu, W. L.; Fanconi, B. M.; Lan, J. K.; Cheng, Y. L.; Liou, H. C.; Wang, Y. L.; Feng, M. S.; Chao, C. G. J Electrochem Soc 2001, 148, F195.